Front. Chem. China 2007, 2(4): 359–363
DOI 10.1007/s11458-007-0068-7

RESEARCH ARTICLE

LIU Qinqin, YANG Juan, SUN Xiujuan, CHENG Xiaonong

Preparation and characterization of $ZrWMoO_8$ powders with different morphologies

Abstract $ZrWMoO_8$ powders with different morphologies were obtained using ammonium tungstate, molybdate tungstate and zirconium tungstate as the starting materials by dehydrating the precursor $ZrWMoO_7(OH)_2(H_2O)_2$. The precursor was studied by thermo-gravimetric and differential scanning calorimetry (TG-DSC). The influence of the gelling agents (HCl, $HClO_4$, HNO_3, H_2SO_4 and H_3PO_4) on the crystallization process and crystal morphology of the products prepared was investigated by X-ray powder diffraction (XRD), scanning electron micrograph (SEM) and X-ray fluorescence spectrometer (XRF). Results showed that the morphology of the $ZrWMoO_8$ particles can be simply adjusted by changing the gelling agents, and the thermal expansion coefficients of cubic $ZrWMoO_8$ prepared in HCl solution are -3.84×10^{-6} K^{-1} from 100°C to 700°C.

Keywords negative thermal expansion, $ZrWMoO_8$, dehydration, precursor

1 Introduction

Negative thermal expansion (NTE) materials have received considerable attention since the NTE material ZrW_2O_8 had been reported by Evans et al. [1–3] in 1995. The NTE materials are mainly utilized to synthesize composite materials with tunable thermal expansion properties, which show potential application in many fields, such as optics, optical fiber communication, medicine materials, low temperature sensor, and so on [4,5].

An ideal NTE material used in the composite materials should possess properties as follows: isotropic NTE property over a wide temperature range including room temperature, accessible from cheap raw materials and easy to prepare, thermodynamically stable and no phase transition over the NTE temperature range. α-ZrW_2O_8 is one of the widely investigated NTE materials which exhibit NTE property in the temperature range of 273–1,050 K, but its thermal expansion curve shows a discontinuity around 430 K which caused by α to α phase transition (from -8.8×10^{-6} to -4.9×10^{-6} K^{-1}). Moreover, α to γ phase transition at 0.21 GPa limited its application in the composite materials under the conditions of high temperature and higher pressure [6–8]. ZrW_2O_8 is usually prepared by solid state method or sol-gel method, and the morphology of the powders prepared is irregular, which may cause stress concentration when it is used in the composite materials. However, the solid solution $ZrW_{2-x}Mo_xO_8$ ($0 \leqslant x < 1.5$) undergoes α to β phase transition below room temperature and α to γ phase transition under higher pressure, which makes it more suitable in preparing composite materials [9].

Clearfield and Blessing [10] reported a new method for preparing $ZrMo_2O_7(OH)_2(H_2O)_2$ in 1972 and from then, cubic $ZrW_{2-x}Mo_xO_8$ can be synthesized by dehydrating the precursor $ZrW_{2-x}Mo_xO_7(OH)_2(H_2O)_2$. Compared with conventional solid state method, this new method can prevent the volatilization of the W/Mo efficiently, and the products prepared have small particle size, high purity and high thermal stability. The application of the NTE materials is greatly influenced by its morphology. Lind et al. [11] had reported that the kind of gelling agents will influence the morphology of the products prepared when the precursor dehydration method is utilized to prepare $ZrMo_2O_8$. In recent years, Sleight [12] had successfully synthesized $ZrW_{2-x}Mo_xO_8$ ($0 \leqslant x < 1.5$) by hydrothermal method and Zhao et al. [13] had prepared $ZrW_{1.7}{}^{VII}W_{0.3}{}^{VI}O_7H_{0.3}(OH)_2(H_2O)_2$ by an improved hydrothermal method, but there are no reports on the morphology control of the $ZrW_{2-x}Mo_xO_8$. In this paper, $ZrWMoO_8$ powders with different morphologies were synthesized by altering the kind of the gelling agents and the refluxing time. The NTE properties of the products prepared were also studied.

Translated from *Chemical Journal of Chinese University*, 2007, 28(3): 397–401 [译自: 高等学校化学学报]

LIU Qinqin, YANG Juan, SUN Xiujuan, CHENG Xiaonong (✉)
School of Material Science and Technology, Jiangsu University, Zhenjiang 212013, China
E-mail: xncheng@ujs.edu.cn

2 Experimental

2.1 Reagents and equipments

Zirconium oxynitrate ($ZrO(NO_3)_2 \cdot 5H_2O$) is AR grade (Rongruida Powder Factory of Zibo City). Ammonium tungstate ($N_5H_{37}W_6O_{24} \cdot H_2O$), ammonium molybdate ($N_5H_{37}Mo_6O_{24} \cdot H_2O$), hydrochloric acid (HCl), perchloric acid ($HClO_4$), sulfuric acid (H_2SO_4) and phosphoric acid (H_3PO_4) are all AR grade (Chemical Reagent Limited Company of Chinese Medicine Group).

Thermal analyzer (NETZSCH STA-449C, Germany) with heating rate of 10°C/min. X-ray powder diffractometer (Rigaku D/max2500, Japan), using Cu target, Kα radiation ($\lambda = 0.154\ 18$ nm). Scanning electron microscopy (Rigaku D/max2500, Japan). X-ray fluorescence spectrometer (ARL9800XP, Switzerland).

2.2 Preparation

6 mol/L HCl, $HClO_4$, HNO_3, H_2SO_4 and H_3PO_4 solution and the mixed solution of H_2SO_4/HCl with the volume ratio of 1 : 1 and 1 : 10 were prepared, respectively. $ZrO(NO_3)_2 \cdot 5H_2O$, $N_5H_{37}W_6O_{24} \cdot H_2O$ and $N_5H_{37}Mo_6O_{24} \cdot H_2O$ were dissolved separately in distilled water according to the mole ratio. First, the W and Mo-containing solution was mixed, and then the Zr-containing solution and the mixed solution were added drop-wise to 15 mL distilled water under vigorous stirring, and the white precipitate was obtained. After stirring for 10 h, 40 mL of the pre-prepared acid was added to the above solution with continuous stirring for serial hours. Finally, the mixture was refluxed for 72 h and aged at room temperature for seven days, followed by washing with distilled water and drying. The solid products obtained were heat-treated at an appropriate temperature between 500°C–550°C to prepare cubic $ZrWMoO_8$ powders.

3 Results and discussion

3.1 Thermo-gravimetric and differential scanning calorimetry (TG-DSC) analysis of precursors

The TG-DSC curves of precursors prepared by different kind of acids as gelling agent are shown in Fig. 1. There is an obvious endothermic peak in DSC curves of all the precursors during the temperature between 100°C–250°C with an evident weight loss in the TG curves, which caused by desorption of structural water. There are two exothermic peaks in DSC curves of precursors prepared by HCl, $HClO_4$ and HNO_3 as gelling agent during the temperature between 230°C–850°C with no obvious weight loss in TG curves, corresponding to the crystallization of cubic $ZrWMoO_8$ and trigonal $ZrWMoO_8$, respectively. However, there is only one exothermic peak at 699.3°C in DSC curve of precursor prepared by H_2SO_4 as gelling agent (in Fig. 1(d)), corresponding to the crystallization of trigonal $ZrWMoO_8$. These results are all coincident with the results of heat-treatment.

3.2 X-ray powder diffraction (XRD)s analysis

The XRD patterns of precursors prepared by different kind of acids as gelling agent are shown in Fig. 2. The XRD pattern of precursors prepared by HCl, $HClO_4$, HNO_3 and HCl/H_2SO_4 mixed acid as gelling agent is shown in Fig. 2(a), which can be indexed to pure $ZrW_2O_7(OH)_2(H_2O)_2$ (JCPDS 27-0994). The results of the X-ray fluorescence spectrometer (XRF)

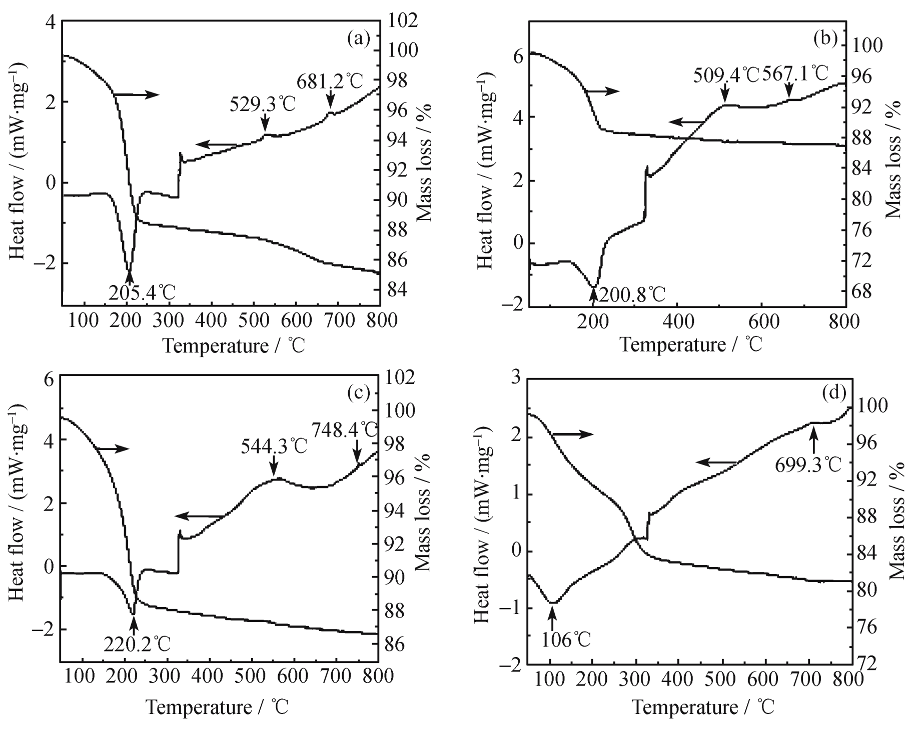

Fig. 1 TG-DSC curves of the precursors prepared by different gelling agents
(a) HCl; (b) HNO_3; (c) $HClO_4$; (d) H_2SO_4

experiment confirmed that the precursor was composed of Zr, Mo and W, etc. and W/Mo molar ratio is approximate to 1 : 1. The above precursors can be transformed to cubic $ZrWMoO_8$ after heat-treatment. The XRD pattern (in Fig. 2(b)) of precursor prepared by H_2SO_4 as gelling agent was both of amorphous and $ZrWMoO_7(OH)_2(H_2O)_2$, and it can only be transformed to trigonal $ZrWMoO_8$ after heat-treatment. The XRD pattern of precursor prepared by H_3PO_4 as gelling agent is shown in Fig. 2(c), which can be indexed to pure $(NH_4)_3PO_4(MoO_3)_{12}(H_2O)_4$ (JCPDS 09-0412), and it can not be transformed to $ZrWMoO_8$ after heat-treatment.

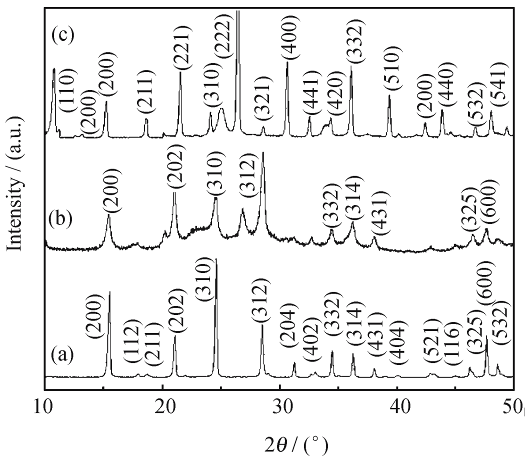

Fig. 2 XRD patterns of the precursors prepared by different gelling agents. (a) HCl, $HClO_4$, HNO_3, HCl/H_2SO_4 mixed acid; (b) H_2SO_4; (c) H_3PO_4

The XRD patterns of the products obtained after heat-treatment at different temperatures are shown in Fig. 3. The XRD pattern of the products prepared by HCl, HNO_3, $HClO_4$ and HCl/H_2SO_4 mixed acid as gelling agent after calcination at 510°C, 530°C and 550°C for 8 h are shown in Fig. 3(a), corresponding to β-ZrW_2O_8, while no obvious diffraction peaks arising from the possible impurity phases, such as WO_3, ZrO_2 etc. Therefore, it can be indexed as cubic $ZrWMoO_8$. The crystallized cubic $ZrWMoO_8$ will be transformed to trigonal $ZrWMoO_8$ after heat-treatment at 750°C for 12 h (in Fig. 3(b)). After further heat-treatment at 850°C for 10 h, the mixture of trigonal $ZrWMoO_8$,WO_3 and ZrO_2 were detected in the XRD pattern as shown in Fig. 3(c), indicating the decomposition of $ZrWMoO_8$. In the experiments, it was found that for different gelling agents, the appropriate temperature to obtain pure $ZrWMoO_8$ with cubic phase was different, which was in agreement with the TG-DSC results as discussed above.

3.3 Scanning electron micrograph (SEM) analysis

Figure 4 shows the morphologies of $ZrWMoO_7(OH)_2(H_2O)_2$ powders obtained with different refluxing time (15 min, 1.5, 2.5 and 12 h) using HCl as gelling agent. It can be seen that after refluxing for 15 min, the particles obtained were short

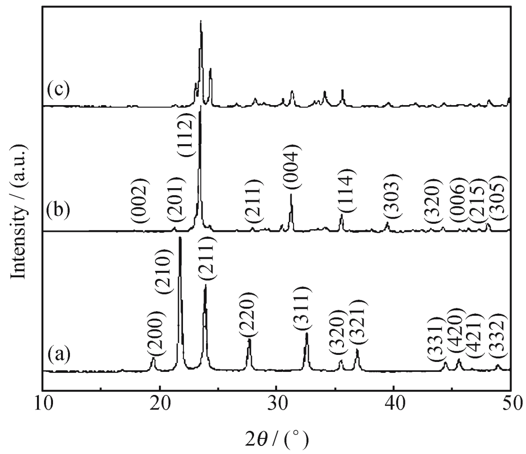

Fig. 3 XRD patterns of powders prepared after calcination at different temperatures. (a) cubic $ZrWMoO_8$; (b) trigonal $ZrWMoO_8$; (c) trigonal $ZrWMoO_8$; ZrO_2 and WO_3

rod-like with average size about 200 nm × 500 nm. The particles grow up during the refluxing process as shown in Fig. 4(b)–(d)). After refluxed for 1.5 and 2.5 h, the particle sizes were 200 nm × 700 nm and 0.2 μm × 1 μm, respectively. The rod-like particles with size of 0.2 μm × 2 μm can be obtained after refluxed for 12 h. The SEM results indicate that the particle only grow up along c axis after refluxing for 15 min and it can also be illustrated that HCl solution will accelerate the $ZrWMoO_7(OH)_2(H_2O)_2$ particle to grow up along c axis.

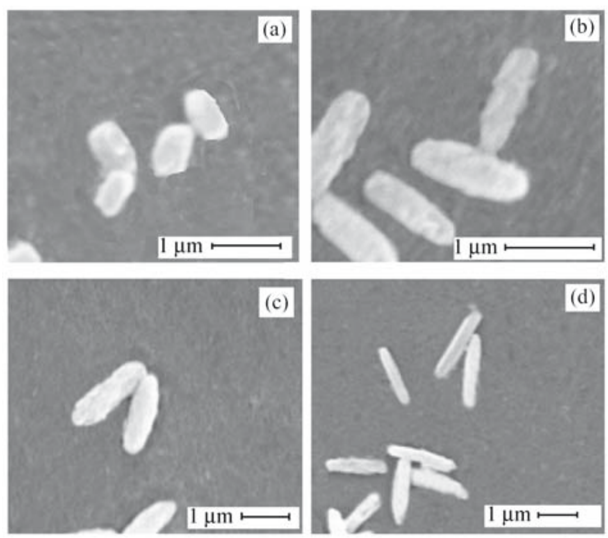

Fig. 4 SEM images of the precursors prepared in HCl solution with different refuxing times. (a) 15 min; (b) 1.5 h; (c) 2.5 h; (d) 12 h

The SEM images of the cubic $ZrWMoO_8$ prepared with different acids as gelling agent are shown in Fig. 5. As shown in Fig. 5(a), the size of the rod-like cubic $ZrWMoO_8$ powders prepared with HCl as gelling agent was 0.2 μm × 2 μm, with

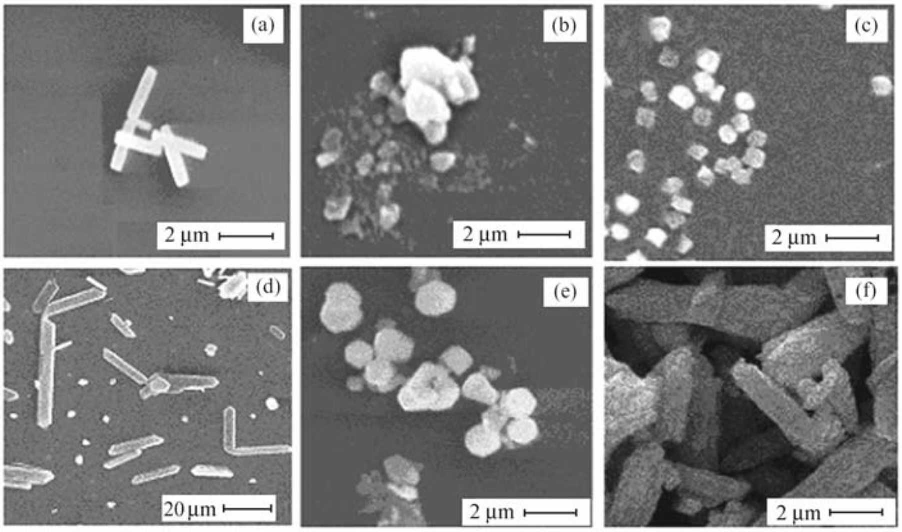

Fig. 5 Morphologies of $ZrWMoO_8$ prepared by different acids
(a) HCl; (b) HNO_3; (c) $HClO_4$; (d) H_2SO_4; (e) H_2SO_4/HCl volume ratio of 1 : 1; (f) H_2SO_4/HCl volume ratio of 1 : 10

no obvious difference compared with the precursor, which suggests that the dehydration process of the precursors has little effect on the morphology of the final products. The morphology of the powders prepared with HNO_3 as gelling agent is irregular (in Fig. 5(b)), while cubic $ZrWMoO_8$ with cuboid morphology can be prepared with $HClO_4$ as gelling agent (in Fig. 5(c)). The sheet crystal trigonal $ZrWMoO_8$ with size of 20–40 μm can be prepared with H_2SO_4 as gelling agent (in Fig. 5(d)). The SEM images of cubic $ZrWMoO_8$ prepared by using H_2SO_4/HCl mixed acid solution with volume ratio of 1 : 1 and 1 : 10 are shown in Fig. 5(e) and (f), respectively. It can be seen that the morphology of product prepared is spheric when H_2SO_4/HCl volume ratio fixed at 1 : 1, while rod-like $ZrWMoO_8$ will be obtained when HCl volume ratio is increased, which further confirmed that HCl will accelerate $ZrWMoO_8$ to grow up along c axis.

3.4 High temperature XRD analysis

The XRD patterns of cubic $ZrWMoO_8$ prepared with HCl as gelling agent after further heat-treatment at different temperatures are shown in Fig. 6 (using 2% α-Al_2O_3 as interior standard). It can be seen that all the diffraction peaks can be indexed to cubic $ZrWMoO_8$ in the temperature range 25°C–700°C without any phase transition. It can also be clearly seen that main peaks of cubic $ZrWMoO_8$ at 2θ of 21.689° and 23.788° move to lower angle along with the increase in the temperature during 25°C–100°C and move to higher angle after 100°C in the partial enlarged drawing. The results indicate that the lattice constant of cubic $ZrWMoO_8$ will increase with the increase in the temperature during 25°C–100°C and exhibit positive thermal expansion property. However, the lattice constant of cubic $ZrWMoO_8$ decreases with the increase in the temperature during 100°C–700°C and exhibit negative thermal expansion property. Sleight et al. [14] had reported that the lattice volume of cubic ZrW_2O_8 shrink by 10% when water molecule exists in the framework. The cubic $ZrWMoO_8$ was obtained by heat-treatment of the precursor $ZrWMoO_7(OH)_2(H_2O)_2$ prepared through liquid solution method in this paper. Therefore, the water molecule also exists in the framework, and this hypothesis process is confirmed by the TG-DSC results shown in Fig. 7. There are two continuous endothermic peaks in DSC curve at 86.3°C and 96.6°C with weight loss about 0.94% in TG curve, which might be caused by the desoption of the water. These results are coincidence with the high temperature XRD results that cubic $ZrWMoO_8$ show negative thermal expansion property after desorption of water at 100°C.

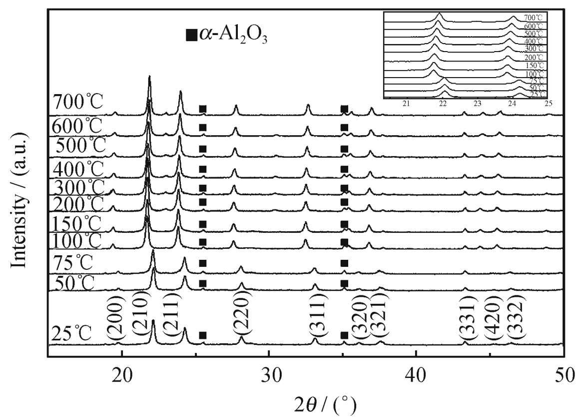

Fig. 6 XRD patterns of $ZrWMoO_8$ collected at different temperatures

3.5 Measurement of thermal expansion constant

The lattice constants of cubic $ZrWMoO_8$ at different temperatures are collected by XRD and calculated by PowderX software [15]. The lattice constant of $ZrWMoO_8$ at room temperature is 0.898 22 nm, which is lower than the value of

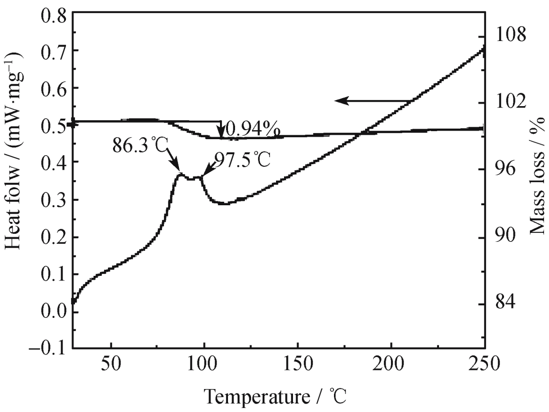

Fig. 7 TG-DSC curves of cubic $ZrWMoO_8$

literature (0.916 73 nm) [4], and it is due to the existence of water in $ZrWMoO_8$. The relationship between cell parameters and temperature in the range of 100°C–700°C was shown in Fig. 8. The lattice constant of cubic $ZrWMoO_8$ decreases with the increase in the temperature, and it exhibits negative thermal expansion property. The average thermal expansion coefficient during whole temperature range was -3.84×10^{-6} K^{-1}, which was correspondence with the thermal expansion coefficient of β-ZrW_2O_8 (-4.9×10^{-6} K^{-1}) during 180°C–700°C after linear fitting ($R = -0.994$, SD $= 6.851 \times 10^{-5}$) [16].

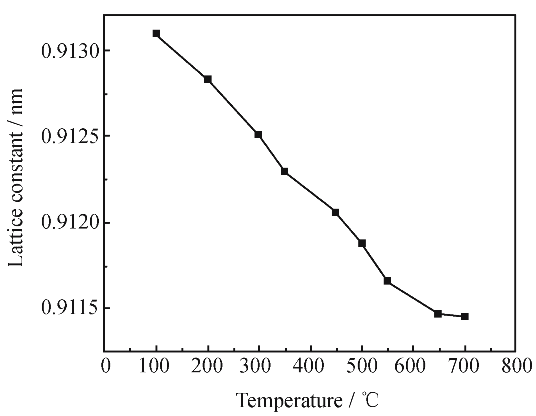

Fig. 8 Lattice constant of $ZrWMoO_8$ as a function of temperature

4 Conclusion

Cubic $ZrWMoO_8$ powders with rod-like, cubic-like and sphere morphology were prepared with the precursor dehydration method by using HCl, $HClO_4$, H_2SO_4/HCl mixed acid (volume ratio fixed at 1 : 1) as gelling agent, and the mechanism is not clear at this moment and needs further investigation. Cubic $ZrWMoO_8$ powders prepared with HCl as gelling agent shows excellent negative thermal expansion property, and the thermal expansion coefficient is -3.84×10^{-6} K^{-1} from 100°C to 700°C.

References

1. Yamamura Y, Nadajima N, Tsuji T. Heat capacity anomaly due to the α-to-β structural phase transition in ZrW_2O_8. Solid State Commu, 2000,114: 453–455
2. Mary T A, Evans J S O, Vogt T. Negative thermal expansion from 0.3-1.50 Kelvin in ZrW_2O_8. Science, 1996, 272: 90–92
3. Kameswari U, Sleight A W, Evans J S O. Rapid synthesis of ZrW_2O_8 and related phase, and structure refinement of $ZrWMoO_8$. Inter J Inorg Mater, 2000, 2: 333–337
4. Evans J S O, Hanson P A, Ibberson R M. Low-temperature oxygen migration and negative thermal expansion in $ZrW_{2-x}Mo_xO_8$. J Am Chem Soc, 2000, 122: 8,694–8,699
5. Zhao Xinhua. The synthesis and structure of $Al_2Mo_{(3x)}W_xO_{12}$. Chem J Chinese Universities, 1999, 20(3): 339–343 (in Chinese)
6. Yasuhisa Y, Toshihide T, Kazuya S. Heat capacity and order-disorder phase transition in negative thermal expansion compound ZrW_2O_8. J. Chem Thermodynamics, 2004, 36: 525–531
7. Evans J S O, Mary T A, Sleight A W. Negative thermal expansion in a large molybdate and tungstate famiy. J Solid State Chem, 1997, 133: 580–588
8. Tao J Z, Sleight A W. The role of rigid unit modes in negative thermal expansion. J Solid State Chem, 2003, 173: 442–448
9. Alexandra K A, Hammonds K D, Dove M T, Pryde A K A, Heine V, Gale J D, Warren M C. Origin of the negative thermal expansion in ZrW_2O_8 and ZrV_2O_7. J Phys Condens Matter, 1996, 8: 10,973–10,982
10. Clearfield A, Blessing R H. The preparation and crystal structure of a basic zirconium molybdate and its relationship to ion exchange gels. J Inor Nucl Chem, 1972, 34: 2,643–2,648
11. Lind C, Wilkinson A P, Rawn C J. Preparation of the negative thermal expansion material cubic ZrW_2O_8. J Mater Chem, 2001, 11: 3,354–3,359
12. Sleight A W. Solution method for making molybdate and tungstate negative thermal expansion material and compound made by the method. UP 6 183 716, 2001
13. Zhao Huaizhou, Zhao Xinhua, Han Buxing. Synthesis and characterization of $ZrW_{1.7} \sim VIW_{0.3} \sim VO_7H_{0.3}(OH)_2 \cdot 2H_2O$. Chem J Chinese Universities, 2004, 25(6): 1,005–1,009 (in Chinese)
14. Duan N, Kameswari U, Slight A W. Further contraction of ZrW_2O_8. J Am Chem Soc, 1999, 121: 10,432–10,433
15. Dong C. Powder X: Windows-95-based program for powder X-ray diffraction data Procession. J Appl Cryst, 1999, 32: 838
16. Evans J S O, Mary T A, Vogt T. Negative thermal expansion in Zr and HfW_2O_8. Chem Mater, 1996, 8: 2,809–2,823